Downstream Effect on Submerged Flow in Rectangular Compound Section Flumes

1 author:
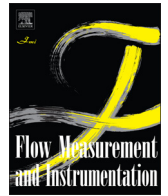
I. A. Al-Khatib

Birzeit University

73 PUBLICATIONS   **204** CITATIONS

Effect of the downstream transition region of a flow measurement flume of rectangular compound cross section on flow properties

Mustafa Gogus [a], Issam A. Al-Khatib [b,*], Ahmet E. Atalay [c]

[a] Hydraulics Division, Civil Engineering Department, Middle East Technical University, Ankara, Turkey
[b] Institute of Environmental and Water Studies, Birzeit University, P.O. Box 14, Birzeit, West Bank, Palestine
[c] Hydraulics Laboratory, Civil Engineering Department, Middle East Technical University, Ankara, Turkey

ARTICLE INFO

ABSTRACT

In this study, the effect of the downstream expansion region of a flow measurement flume of rectangular compound cross section on some of the flow properties; such as the discharge coefficient, C_d, the approach velocity coefficient, C_v and the modular limit, ML were investigated. For this reason, extensive laboratory tests were conducted with nine models of different downstream transitions. The aforementioned hydraulic quantities were then related with the relevant parameters to obtain sets of curves from which one could decide which kind of downstream transition type would produce the highest modular limit. It was found that model type A yielded the highest modular limit with a downstream slope of about 1/7.

1. Introduction

The need for measuring the discharge in streams and rivers arises from the value of water for different uses in the community. By time, the availability of water becomes increasingly important to mankind. Knowledge of the quantity available is the first stage in the efficient management of this vital resource [1–3].

Many studies related to the different types of flow measuring structures of open channels have been done by various investigators [4–12]. In all these studies theoretical analysis were followed by experimental investigations to obtain relations between the relevant quantities.

The head–discharge relations for flows over broad-crested weirs and sharp-crested weirs with a simple cross-section shape, such as truncated triangular, triangular, rectangular, trapezoidal, and others have been studied by many researchers [13–19]. Some useful empirical discharge equations for these weirs have been proposed. In hydraulic engineering, a compound cross-sectional weir composed of triangular and/or rectangular cross section is also a common device for flow control in mountainous gullies and canals [20,21]. Regarding construction, the compound weir could be used to measure the flow discharge providing that the discharge equation of the weir is available [18].

Long-throated flumes provide flexible and economical flow measurement capabilities for a wide variety of open-channel flows. Main advantages include low construction cost, minimal head loss, ability to measure wide ranges of flows with custom-designed structures and adaptability to a variety of channel types section [22,23].

Long-throated flumes of rectangular compound cross sections have a main channel at the bottom of the flume that is narrower than the width of the upper cross section (Fig. 1), where B is the bottom width of the approach channel, b the bottom width of the control section, B_0 the top width of head measurement section, g the acceleration of gravity, H the total energy head, h_1 the gauged head at upstream head measurement section, H_1 the total energy head at upstream head measurement section, L_{ap} the length of the approach channel, L_{ct} the length of the converging transition, L_{dt} the length of the diverging transition, L_{ent} the length of the entrance channel, L_{thr} the length of the throat in the direction of flow and Q the volumetric rate of flow. This results in the pass of sediment carried by the flows and for producing a readable and stable water surface at the gauging station.

The head–discharge equations for long throated flumes are simply obtained by applying the energy equation between the head measurement section and the control section. A number of assumptions are made for the sake of simplicity, and therefore, must be adjusted for real fluids by introducing a coefficient. Regardless of the throat cross section, the equation has the form

$$Q = C_d K H_1^u \tag{1}$$

where Q is the volumetric flow rate; K the coefficient depending on the size and shape of the weir; and u the dimensionless

* Corresponding author. Tel./fax: +972 2 2982120.
  E-mail addresses: ikhatib@birzeit.edu, ikhatib2012@yahoo.com (I.A. Al-Khatib).

Nomenclature

A^*	imaginary wetted area at control section if water depth were equal to h_1
A_c	cross-sectional area at control section.
A_1	cross-sectional area of flow at head measurement section.
$A\text{-}S_i$	type A models tested with various downstream slopes. The subscript i denotes the downstream slopes (vertical: horizontal) of type A models as $i = 1/0, 1/1, 1/3, 1/5$, and $1/7$
B	bottom width of the approach channel
b	bottom width of the control section
B_c	top width at the control section
B_0	top width of head measurement section
$B\text{-}S_j$	type B models tested with various downstream slopes. The subscript j denotes the downstream slopes (vertical: horizontal) of type B models as $j = 1/1, 1/3, 1/5$, and $1/7$
C_d	discharge coefficient
C_v	approach velocity coefficient
g	acceleration of gravity
H	total energy head
h	gauged head
H_1	total energy head at upstream head measurement section
H_2	downstream sill-referenced energy head is the available head loss over the structure
$H_{1(101)}$	total energy head at upstream head measurement section corresponding to modular limit
$H_{1(100)}$	total energy head at the head measurement section for the free-flow case
H_2	total energy head at downstream head measurement section
h_1	head at upstream head measurement section
$h_{1(101)}$	head at upstream head measurement section corresponding to modular limit
h_2	measured head at downstream head measurement section
K	coefficient depending on the size and shape of the weir
L_{ap}	length of the approach channel
L_{ct}	length of the converging transition
L_{dt}	length of the diverging transition
L_{ent}	length of the entrance channel
L_{thr}	length of the throat in the direction of flow
ML	modular limit
Q	volumetric rate of flow
Q_{pred}	predicted volumetric rate of flow
Q_{mea}	measured discharge
ΔQ	absolute value of the difference between the measured discharge, Q_{mea} and Q_{pred}
$Q_{(100)}$	discharge corresponding to $H_{1(100)}$
$Q_{(101)}$	volumetric rate of flow corresponding to modular limit
u	dimensionless number depending on the shape of the cross section of the control section
V	average flow velocity
y_c	critical water depth at control section
Z	step height
α	energy correction coefficient for the head measurement section

number depending on the shape of the cross section of the control section, which is equal to 3/2 for rectangular cross sections [24] and C_d the discharge coefficient and is introduced to correct for a number of assumptions; for example, absence of energy losses between the control and head measurement section, uniform velocity distribution in these two sections, and straight parallel streamlines across the flume sections considered. It is a coefficient mainly governed by H_1/L_{thr}.

In open channel flows, it is seldom practical to measure the total energy head, H_1, directly. It is a common practice to relate the flow rate to the upstream sill referenced head, h_1, in the following form [25–27]:

$$Q = C_d C_v K h_1^{3/2} \qquad (2)$$

where C_v is the approach velocity coefficient, which corrects for neglecting the velocity head at the measurement section.

The purpose of this study is to investigate the effect of the downstream transition region of a flow measurement flume of rectangular compound cross section on the discharge coefficient, approach velocity coefficient, and modular limit, and eventually to determine the optimum downstream slope which will yield the maximum modular limit.

2. Present study

2.1. Discharge coefficient, C_d

From Fig. 1, assuming that energy losses between the head measurement section and the control section are negligible, velocity distributions are uniform, and all streamlines are straight and parallel to each other; applying the energy and continuity equations, and considering the flow through the control section is critical, one can derive the general equation of the critical flow as
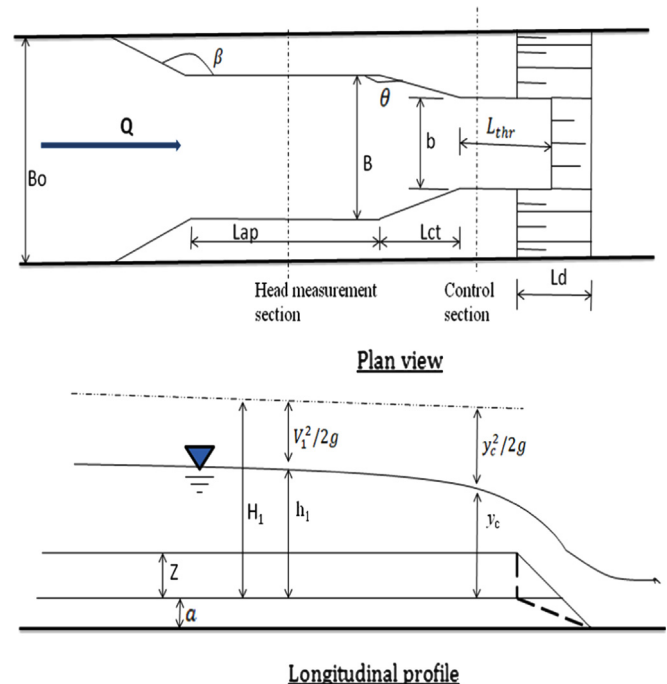

Fig. 1. Definition sketch of flow measurement flume of compound cross section used in the theoretical analysis (—— Model A, – – – – Model B).
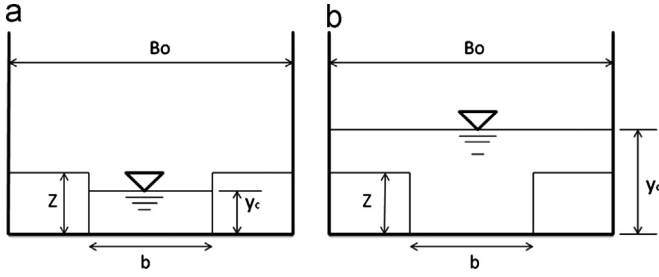
Fig. 2. Two different flow cases through flume section: (a) Case 1 and (b) Case 2.

given below

$$Q = \left[\frac{gA_c^3}{B_c}\right]^{1/2} \tag{3}$$

where A_c and y_c are the cross-sectional area and critical flow depth at the control section, respectively; B_c the top width at the control section. For flumes of rectangular compound cross section, there are two different cases to be analyzed, at the control section, as shown in Fig. 2.

Case 1. ($h_1 \leq Z$, $y_c < Z$, $B_0 = b$)

For Case 1, flow occurs only through the lower part of the compound cross section. For this case, the equation of discharge can be obtained as [25–28]

$$Q = \frac{2}{3}b\left(\frac{2}{3}g\right)^{1/2}H_1^{3/2} \tag{4}$$

Case 2. ($h_1 > Z$, $y_c > Z$)

In this case, flow occurs through the compound cross section, so that the depth at the control section, i.e., the critical depth, is greater than Z. The area of the flow at the control section is

$$A_c = bZ + (y_c - Z)B_0 \tag{5}$$

where $B_0 =$ top width of the head measurement section.

Applying the energy and continuity equations as in the previous case and rewriting Eq. (3) gives [25–27]

$$Q = \left(\frac{g}{B_0}\right)^{1/2}\left[bZ + B_0\left(\frac{2}{3}H_1 - \frac{bZ}{3B_0} - \frac{2Z}{3}\right)\right]^{3/2} \tag{6}$$

Eqs. (4) and (6) are based on a number of idealized assumptions, such as uniform velocity distribution at the head measurement and the control sections, straight and parallel streamlines at both sections and the absence of energy losses between the head measurement and control sections. In reality, these assumptions are not entirely true and accounted for by the introduction of the discharge coefficient, C_d. Moreover, in an open channel flow it is not practical to measure the energy head H_1 directly. It is a common practice to relate the flow rate to the upstream sill-referenced water level, h_1, by introduction of the approach velocity coefficient, C_v, which corrects for neglecting the velocity head in the head measurement section. Then, the equations of discharge take the final forms

$$Q = \frac{2}{3}C_dC_vb\left(\frac{2}{3}g\right)^{1/2}h_1^{3/2} \tag{7}$$

and

$$Q = C_dC_v\left(\frac{g}{B_0}\right)^{1/2}\left[bZ + B_0\left(\frac{2}{3}h_1 - \frac{bZ}{3B_0} - \frac{2Z}{3}\right)\right]^{3/2} \tag{8}$$

In the literature the value of the discharge coefficient, C_d, is in general related to the dimensionless ratio H_1/L_{thr} where L_{thr} is the throat length. The effect of energy losses due to friction between the head measurement and control sections on C_d becomes evident in the form of decreasing discharge coefficient as H_1/L_{thr} decreases [8,28]. When the sill-referenced head is small with respect to the crest length, the thin layer of water above the sill is very close to the rough boundary, and as a result, energy loss due to friction is a relatively large part of H_1. In addition to that, for smaller H_1/L_{thr}, the effect of curvature on the discharge coefficient is stronger. The values of the discharge coefficient, C_d, can be computed from Eqs. (9) and (10) for the experiments of Cases 1 and 2, respectively

$$C_d = \frac{3}{2}\frac{Q}{b((2/3)g)^{1/2}H_1^{3/2}} \tag{9}$$

$$C_d = \frac{Q(B_0/g)^{1/2}}{[bZ + B_0((2/3)H_1 - (bZ/3B_0) - (2Z/3))]^{3/2}} \tag{10}$$

2.2. Approach velocity coefficient, C_v

The values of C_v are determined from Eq. (11) for $y_c \leq Z$ and Eq. (12) for $y_c > Z$

$$C_v = \left(\frac{H_1}{h_1}\right)^{3/2} \tag{11}$$

$$C_v = \left[\frac{bZ + B_0\left(\frac{2}{3}H_1 - \frac{bZ}{3B_0} - \frac{2Z}{3}\right)}{bZ + B_0\left(\frac{2}{3}h_1 - \frac{bZ}{3B_0} - \frac{2Z}{3}\right)}\right]^{3/2} \tag{12}$$

Because the discharge is mainly determined by the wetted area at the control section and the related velocity of approach at the head measurement section, it was convenient to correlate C_v to $\sqrt{\alpha}C_dA^*/A_1$. Here A^* is imaginary wetted area at the control section if the depth of water were equal to h_1; A_1 the cross-sectional area of the flow at the head measurement section; and α the energy correction coefficient for the head measurement section, which is taken as 1.04 [15,28,29]. In the above mentioned relationship of C_v, Bos take the value of α as 1.0 [15]. Determination of A_1 and A^* for the models investigated, Eqs. (13) and (14) were used for $h_1 \leq Z$ and for $h_1 > Z$, respectively, in two distinct cases

$$A^* = bh_1 \text{ and } A_1 = Bh_1 \tag{13}$$

and

$$A^* = bZ + B_0(h_1 - Z) \text{ and } A_1 = BZ + B_0(h_1 - Z) \tag{14}$$

2.3. Modular limit

The difference between the upstream sill-referenced energy head H_1 and the downstream sill-referenced energy head H_2 is the available head loss over the structure and the ratio H_2/H_1, is defined as the submergence ratio of the structure. For low submergence ratios, critical flow occurs on the weir crest and tailwater conditions have no effect on the upstream head and thus on the discharge, so the flow is called *modular*. At very high submergence ratios, critical flow no longer exists on the weir crest, so the upstream sill-referenced head is influenced by the tailwater level and the flow is called nonmodular or submerged. The limiting submergence ratio between modular and nonmodular flows is named the modular limit (ML). It is defined as the submergence ratio value, H_2/H_1, such that real discharge through the weir deviates by 1% from the discharge calculated by the head–discharge equation [28]. While designing a flume in the modular range, ML should be known.

The general relationship between Q and H_1 for any kind of weir or flume in the modular flow range is

$$Q_{(100)} = KH_{1(100)}^{3/2} \tag{15}$$

where $Q_{(100)}$ discharge corresponding to $H_{1(100)}$ which is the total energy head at the head measurement section for the free-flow case.

For nonmodular flow, $Q_{(101)}$ and $H_{1(101)}$ are introduced, where $Q_{(101)}$ discharge deviating 1% from the actually measured discharge and $H_{1(101)}$ corresponding total head at the head measurement section. Then for $y_c \leq Z$ Eq. (16), which reduces to Eq. (17), and for $y_c > Z$ Eq. (18), which reduces to Eq. (19), are obtained

$$\frac{Q_{(101)}}{Q_{(100)}} = 1.01 = \frac{2/3C_d b((2/3)g)^{1/2} H_{1(101)}^{3/2}}{2/3C_d b((2/3)g)^{1/2} H_{1(100)}^{3/2}} \tag{16}$$

$$H_{1(101)} = 1.0067 H_{1(100)} \tag{17}$$

$$\frac{Q_{(101)}}{Q_{(100)}} = 1.01 = \frac{(g/B_0)^{1/2}[bZ + B_0(2/3H_{1(101)} - (bZ/3B_0) - (2Z/3))]^{3/2}}{(g/B_0)^{1/2}[bZ + B_0(2/3H_{1(100)} - (bZ/3B_0) - (2Z/3))]^{3/2}} \tag{18}$$

$$H_{1(101)} = 0.006656\frac{bZ}{B_0} - 0.006656 + 1.006656H_{1(100)} \tag{19}$$

The head at the head measurement section then becomes equal to $h_{1(101)}$ and is defined as

$$h_{1(101)} = H_{1(101)} - \frac{V_1^2}{2g} \tag{20}$$

where V_1 is the average flow velocity at the upstream head measurement section.

3. Experimental setup and experiments

The purpose of this experimental study was to analyze the effect of the type of downstream expansion in a compound rectangular flow measurement flume on the values of C_d, C_v and ML. For this reason a flume of fixed dimensions with nine different downstream transitions were manufactured and assembled to the flume in a row. Totally nine types of flumes with various downstream transitions were tested in the course of this study.

All series of experiments, totally 148 runs were performed in a glass walled laboratory flume 11.0 m long, 0.287 m wide and 0.70 m deep in the Hydromechanics Laboratory of the Middle East Technical University, Ankara, Turkey. The models of which plan view and longitudinal profile are shown in Fig. 1 were manufactured from plexiglass and placed to the almost mid-length of the main channel system. The desired downstream transitions were prepared from steel plates and concrete, and then assembled to the flume. Table 1 shows geometrical properties of the models tested as well as the number of

tests conducted with each model and the ranges of the flow depths at the measurement section and the corresponding discharge ranges. The diversion transition connects the throat to the tailwater channel. The elevation difference between the bottoms of the throat and tailwater channel is eliminated by this transition zone with a height of "$a = 4$ cm". It has variable bottom and side slopes. For model A, the throat was elongated at a required length to have a same slope with the side walls of the throat (Fig. 1). For model B, the throat was not elongated. The end section of the throat and the rectangular compound cross section of step height Z fell on the same vertical plane so that the bottom transition of the throat and its side walls did not have the same slope (Fig. 1). The throat is the control section which is the part of the weir with a rectangular compound cross section over which critical flow occurs. The plan view and the longitudinal profile of the model types tested are shown in Fig. 1. The dimensions of the various models used in the experiments are given in Table 1. The symbols used in the description of the model types, A-S_i and B-S_j ($i = 1/0, 1/1, 1/3, 1/5, 1/7$ and $j = 1/1, 1/3, 1/5, 1/7$), correspond to type A and type B models, respectively. The subscripts i and j denote the downstream slopes (vertical:horizontal) of the same models, respectively.

The approach channel is the part of the main channel which is followed by the converging transition of the flume. The depth of the flow is measured at the head measurement section which is the mid-section of this channel. The tailwater channel is the energy dissipater part where the flow becomes subcritical from supercritical. In the experiments, a range of discharges provided from the constant-head storage tank for a selected model type was measured with a rectangular sharp-crested weir, 26 cm wide and 29 cm high, mounted in the inlet box of the laboratory flume. Two point gauges of 0.01 cm accuracy were installed along the centerline of the model for head measurements. The first was fixed to the mid-section of the approach channel to measure the upstream head, h_1. The second gauge was placed downstream of the model in order to measure the downstream sill-referenced head, h_2, when the tailwater depth was forced to increase during the determination of ML. Depth of the flow above the crest level at approach channel was measured when the tailgate of the flume was fully open (free flow measurements). For the same discharge, the point gauge was set to the value $h_{1(101)}$, which is the flow depth corresponding to a 1% increase in free discharge and obtained from the rating curve of the model. The tailgate of the flume was then raised gradually until the water surface at the measurement section touched the point gauge. At that moment, the depth of the flow in the tailwater channel above the crest elevation was measured and the corresponding H_2 and ML were calculated.

4. Presentation and discussion of results

4.1. Discharge coefficient, C_d

It is obvious that the type of the downstream expansion of the long throated flumes influence the streamline curvature of the

Table 1
Dimensions of the nine different models used in the experiments.

Model type	The number of tests	The range of h_1 (cm)	The range of Q (l/s)	b (cm)	B (cm)	Z (cm)	B_0 (cm)	β (deg)	θ (deg)	L_{ap} (cm)	L_{ct} (cm)	L_{thr} (cm)	L_d (cm)
A-$S_{1/0}$	16	3.81–20.28	1.70–44.33	15.8	19.5	10	28.7	166	173	60	16	12	0
A-$S_{1/1}$	15	4.83–18.67	2.57–40.97	15.8	19.5	10	28.7	166	173	60	16	22	14
A-$S_{1/3}$	15	6.29–19.67	4.03–40.76	15.8	19.5	10	28.7	166	173	60	16	42	42
A-$S_{1/5}$	17	4.87–20.51	2.45–43.78	15.8	19.5	10	28.7	166	173	60	16	62	70
A-$S_{1/7}$	16	3.97–20.50	1.52–42.95	15.8	19.5	10	28.7	166	173	60	16	82	98
B-$S_{1/1}$	18	3.43–17.89	1.43–43.24	15.8	19.5	10	28.7	166	173	60	16	12	14
B-$S_{1/3}$	18	3.57–19.27	1.56–43.24	15.8	19.5	10	28.7	166	173	60	16	12	42
B-$S_{1/5}$	17	3.73–19.87	1.71–43.38	15.8	19.5	10	28.7	166	173	60	16	12	70
B-$S_{1/7}$	16	3.71–20.27	1.57–42.88	15.8	19.5	10	28.7	166	173	60	16	12	98

flow in the control section. Therefore, the effect of the downstream expansion of the long throated flumes on discharge coefficient should be analyzed.

For practical purposes, it is better to relate C_d to h_1/L_{thr}. The reason for that is not to know the value of the approach flow velocity for a flow measurement structure, of which the discharge is to be found from the measured value of h_1.

In order to see the effect of the downstream expansion on the values of the discharge coefficient, C_d, the C_d vs h_1/L_{thr} values are plotted for type A and B models in Figs. 3 and 4, respectively.

In Fig. 3, since the throat length of each type of A model was different, model $A\text{-}S_{1/7}$ had the largest throat length (Table 1), and the C_d values of some of the model types did not have a wide range of h_1/L_{thr}. Some of the data points in this figure are highly scattered, which corresponds to flow conditions at which the measured depth, h_1, was close to step height, Z.

The situation is a little bit different in Fig. 4 because of the constant throat length, the range of h_1/L_{thr} for a given model type

is quit wide. From the analysis of Figs. 3 and 4, it is clearly seen that type A models give higher C_d than type B models for the range of h_1/L_{thr} in between 0.45 and 0.85. It can also be seenthat, for the same h_1/L_{thr} of type B models, as the downstream expansion slope decreases, the discharge coefficient values decrease.

4.2. Approach velocity coefficient, C_v

As mentioned previously, the coefficient C_v is usually expressed as a function of the ratio $\sqrt{\propto} C_d A^*/A_1$. In this study, as done by Bos [15], the parameter α used in the expression of $\sqrt{\propto} C_d A^*/A_1$ was removed. The available C_v data of type A and B models are plotted as a function of $C_d A^*/A_1$ in Figs. 5 and 6. In both figures, all the data points, except a few corresponding to the flow cases of depths around the step height, Z, of the approach channel, fall on a single curve. Therefore, regardless of the type of downstream transition, the flow measurement channels of the compound rectangular cross section yield the same C_v versus $C_d A^*/A_1$ curve.
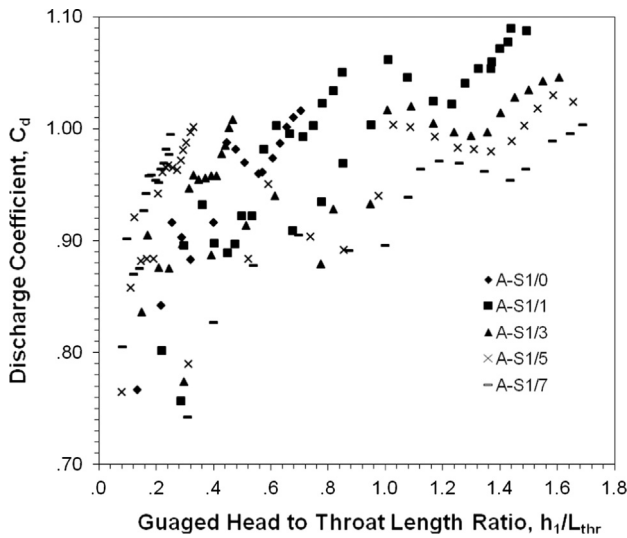

Fig. 3. Variation of the discharge coefficient, C_d, with the approach head to throat length ratio, h_1/L_{thr}, for type A models tested.
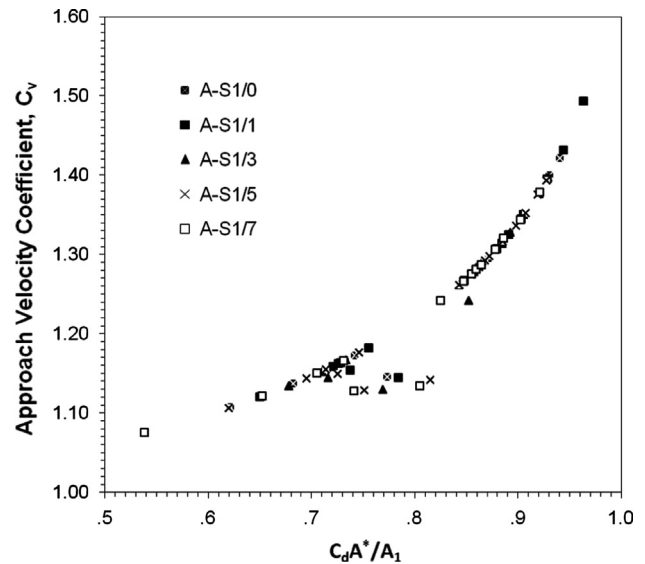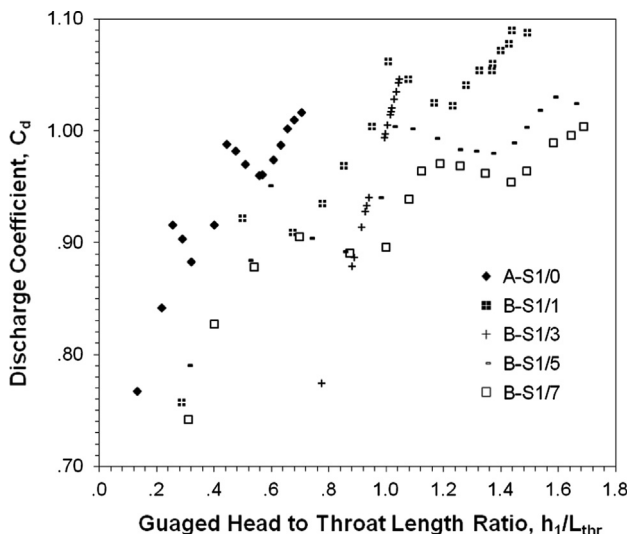

Fig. 5. Variation of C_v versus $C_d A^*/A_1$. for A type models.

Fig. 4. Variation of the discharge coefficient, C_d, with the approach head to throat length ratio, h_1/L_{thr}, for type B models tested.
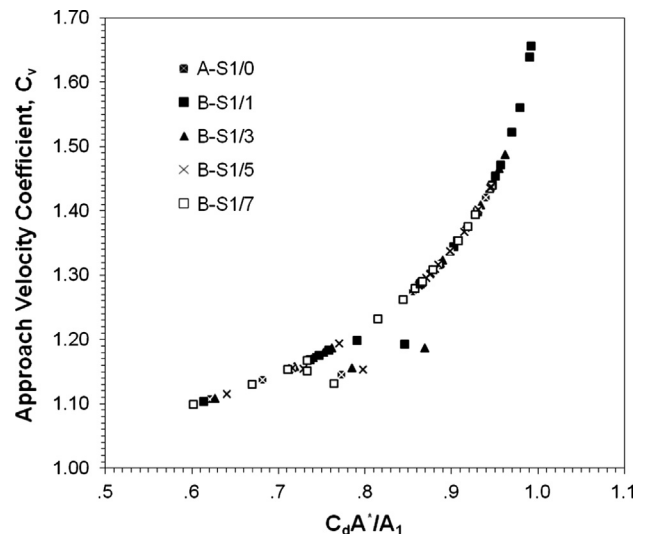

Fig. 6. Variation of C_v vsersus $C_d A^*/A_1$. for the type B models and the type $A\text{-}S_{1/0}$ tested.

4.3. Modular limit

Referring to the dimensional analysis applied to similar type of problem, Hatipoglu [30] showed that ML is related to Froude number of the flow, Fr_1, at the depth measurement section. Figs. 7 and 8 show the variation of ML with Fr_1 for models A-S_i and B-S_i, respectively. As a general trend, in both types of models for a given Fr_1, the modular limit increases and attains its maximum value as the downstream transition slope of the model decreases.

In Fig. 7, it is clearly seen that as the downstream transition slope of the model decreases, the values of the ML of the models get closer to each other and attain maximum values for a given Fr_1. The trend of the data points of models A-$S_{1/5}$ and A-$S_{1/7}$ reveals that may be further decrease to be applied to the downstream transition slope will not change ML values too much. The ML values of A-$S_{1/7}$ are very slightly greater than those of A-$S_{1/5}$ for almost the whole range of Fr_1 tested. It can be predicted that a model type A with a downstream transition slope of 1/6 will also have ML values in between those of models A-$S_{1/5}$ and A-$S_{1/7}$. Therefore in the case of selecting model type A for application in practice, due to the economical reasons the downstream transition

slope of 1/6 can be recommended. This slope is the same as the one proposed by Bos and Reinink [31] for long throated flumes of rectangular cross section. The highest value of the ML obtained among models A-S_i (A-$S_{1/5}$) is about 0.95.

However, Fig. 8 shows that ML values of B-$S_{1/5}$ and B-$S_{1/7}$ for a given Fr_1 are not so much close to each other. The model type of B-$S_{1/7}$ gives the highest value of ML as 0.95 among the other types of model B.

In order to make a comparison between models A and B of the same downstream transition slopes Figs. 9–12 were plotted. From the examination of these figures it can be seen that, except Fig. 12, models A-S_i always give higher ML values for the whole range of Fr_1, tested. In Fig. 12 for Fr_1 greater than about 0.60 data points of both models almost coincide with the highest values of ML as 0.92 and 0.95 for models A and B, respectively. However in the same figure model B gives smaller ML values than those of model A for Fr_1 less than 0.60 since in Fig. 12, in general, model A-$S_{1/7}$ can be recommended against model B-$S_{1/7}$ in practical application. But as it has been stated before, the model A-$S_{1/6}$ will yield almost the same trend for the variation of ML with Fr_1. Therefore, also
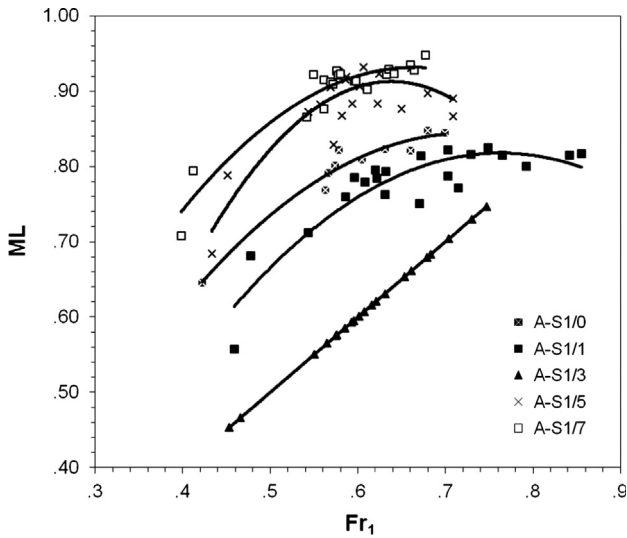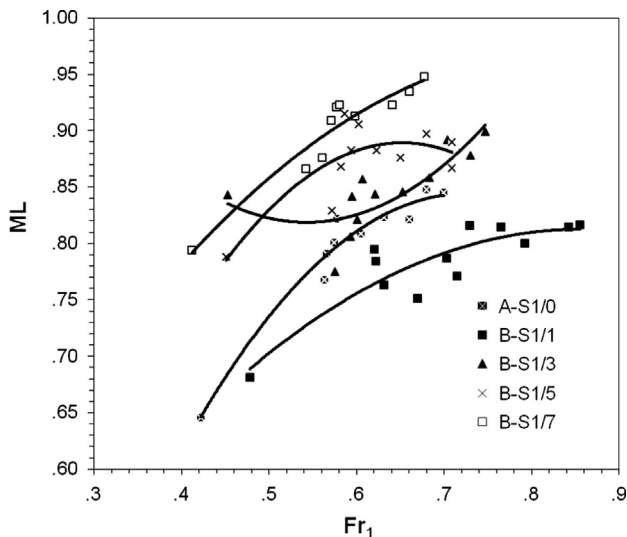

Fig. 7. ML versus Fr_1 for A type models.

Fig. 8. ML versus Fr_1 for the type B models and the type A-$S_{1/0}$ tested.
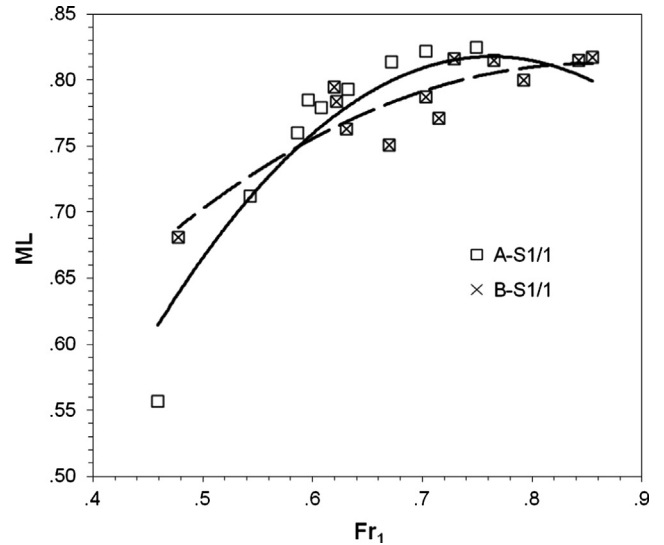

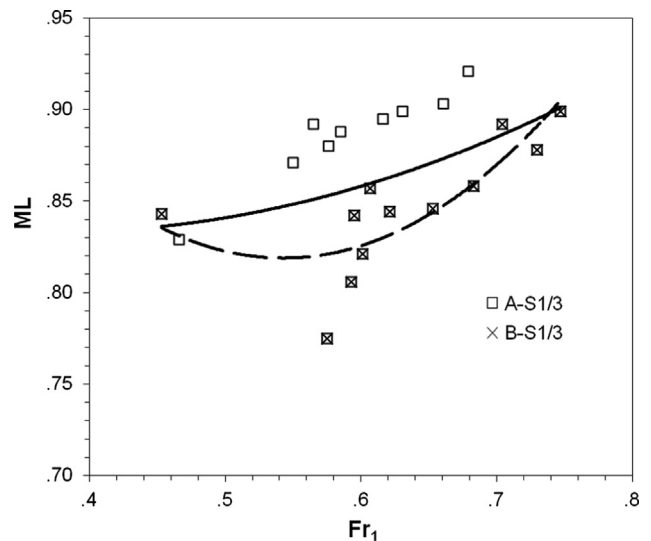**Fig. 9.** ML versus Fr_1 for models A-$S_{1/1}$ and B-$S_{1/1}$.

Fig. 10. ML versus Fr_1 for models A-$S_{1/3}$ and B-$S_{1/3}$.

Fig. 11. *ML* versus Fr_1 for models A-$S_{1/5}$ and B-$S_{1/5}$.

Fig. 12. *ML* versus Fr_1 for models A-$S_{1/7}$ and B-$S_{1/7}$.
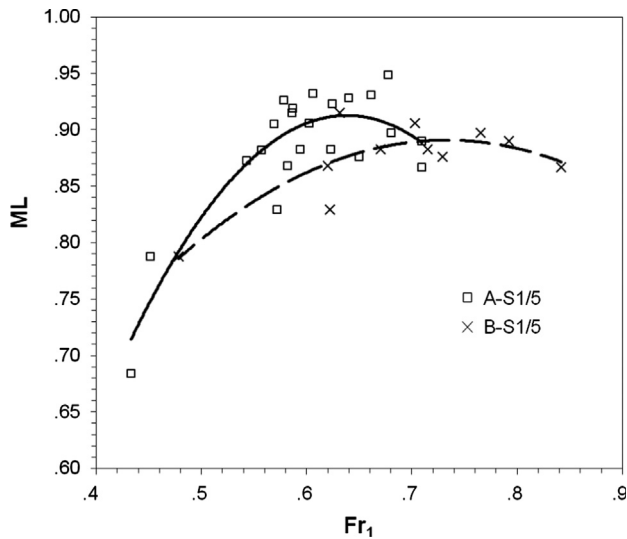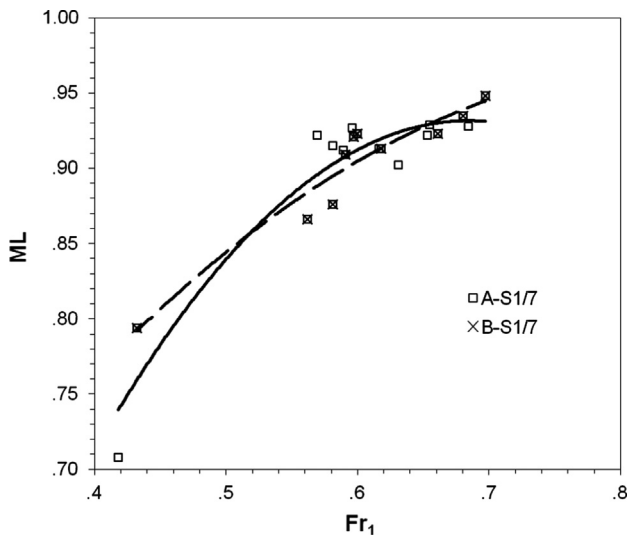
considering the economical aspect of the construction of the structure, the model type A with a downstream transition slope of 1/6 instead of 1/7 can be recommended for application in practice.

As an example to see the results of experiments carried out throughout this study, the related data of model A-$S_{1/7}$ is presented Table 2.

5. Discharge estimation

Using the head–discharge relationship (Eqs. (7) and (8)) for a given head, h_1, at the depth measurement section, the discharge can be estimated if the values of C_d and C_v are known. The C_d and C_v values can be obtained from Figs. 3 to 6 depending on the downstream transition slope. After calculating C_d and C_v values, the predicted discharge, Q_{pred} and the overall error in the prediction of discharge can be estimated from the division of ΔQ, which is the absolute value of the difference between the measured discharge, Q_{mea} and Q_{pred} to Q_{mea}.

6. Conclusions

In this study, a series of laboratory experiments were conducted to investigate the effect of the downstream expansion of flow measuring flumes of rectangular cross section on C_d and C_v. The variation of C_d and C_v with various dimensionless quantities was analyzed, and general equations relating C_d and C_v to these quantities have been derived. From the analysis of these experimental results, the following conclusions can be drawn:

(1) For practical purposes, it is better to relate C_d to h_1/L_{thr} and C_v to $C_d A^*/A_1$.
(2) In type A models, C_d do not have a wide range of h_1/L_{thr}, while h_1/L_{thr} for a given model type B is quit wide.
(3) Type A models give higher C_d values than type B models for a range of h_1/L_{thr} between 0.45 and 0.85.
(4) Flow measurement channels of compound rectangular cross sections regardless of the type of downstream transition yield the same C_v versus $C_d A^*/A_1$ curve.
(5) The value of *ML* increases as the slope of the downstream transition of the models A-S_i and B-S_i decreases.
(6) The model A-$S_{1/7}$ yields the maximum *ML* among the models tested. This model or based on the *ML* data obtained in this

Table 2
Experimental data for model A-$S_{1/7}$.

Q (m³/s)	h_1 (m)	H_1 (m)	C_d (dimensionless)	h_1/L_{thr} (dimensionless)	C_v (dimensionless)	$C_d A^*/A_1$ (dimensionless)	ML (dimensionless)	Fr_1 (dimensionless)
0.0015	0.039	0.042	0.663	0.048	1.075	0.538	0.715	0.315
0.0043	0.068	0.073	0.805	0.083	1.121	0.652	0.708	0.398
0.0064	0.080	0.089	0.902	0.098	1.166	0.731	0.725	0.464
0.0084	0.099	0.109	0.870	0.121	1.150	0.705	0.841	0.441
0.0105	0.116	0.126	0.875	0.142	1.128	0.741	0.842	0.480
0.0133	0.130	0.141	0.927	0.158	1.134	0.805	0.800	0.482
0.0158	0.136	0.150	0.942	0.166	1.242	0.825	0.856	0.522
0.0184	0.144	0.161	0.958	0.175	1.266	0.847	0.922	0.549
0.0207	0.151	0.170	0.959	0.184	1.276	0.855	0.915	0.561
0.0239	0.162	0.183	0.954	0.198	1.281	0.859	0.912	0.569
0.0269	0.171	0.194	0.952	0.209	1.287	0.864	0.927	0.576
0.0298	0.178	0.203	0.964	0.217	1.306	0.878	0.913	0.596
0.0333	0.186	0.215	0.969	0.227	1.320	0.886	0.902	0.611
0.0363	0.192	0.224	0.982	0.234	1.345	0.903	0.922	0.633
0.0397	0.201	0.235	0.977	0.245	1.344	0.902	0.929	0.635
0.0430	0.205	0.244	0.995	0.250	1.378	0.921	0.928	0.664

Note: b = 0.158 m; B = 0.195 m; Z = 0.10 m; B_0 = 0.287 m and L_{thr} = 0.82 m.

study, the model A-$S_{1/6}$ can be recommended for application in practice when considering the economical aspect of the construction of the structure.

References

[1] Bos MG, Clemmens AJ, Replogle JA. Design of long-throated structures for flow measurement. Irrigation and Drainage Systems 1986;l(1):75–91.

[2] Clemmens AJ, Bos MG. Critical depth relations for flow measurement design. Journal of Hydraulic Engineering, ASCE 1992;118(4):640–4.

[3] Bos MG, Wijbenga JHA. Passage of sediment through flumes and over weirs. Irrigation and Drainage Systems 1997;11(1):29–39.

[4] Replogle JA, Clemmens AJ, Tanis SW, McDade JH. Performance of large measuring flumes in main canals. In: Proceedings of the specialty conference on irrigation and drainage surviving external pressures, ASCE. Jackson, Wyoming, USA; 1983. p. 530–7.

[5] Hager WH, Schwalt M. Broad-crested weir. Journal of Irrigation and Drainage Engineering, ASCE, 120; 13–26.

[6] Özkandemir V. Hydraulic characteristics of broad-crested weirs of rectangular compound cross section. Ankara, Turkey: Middle East Technical Univ.; 1997 [MS thesis].

[7] Wahl TL, Replogle JA, Wahlin BT, Higgs JA. New developments in design and application of long-throated flumes. In: Joint conference on water resources engineering and water resources planning & management. Minneapolis, Minnesota: American Society of Civil Engineers; July 30–August 2, 2000.

[8] Johnson MC. Discharge coefficient analysis for flat-topped and sharp-crested weirs. Irrigation Science 2000;19:133–7.

[9] Göğüş M, Defne Z, Özkandemir V. Broad-crested weirs with rectangular compound cross sections. Journal of Hydraulic Engineering, ASCE, 132; 272–280.

[10] Hager WH, Schwalt M. Broad-crested weir. Journal of Irrigation and Drainage Engineering, ASCE 1994;120(1):13–26.

[11] Fritz HM, Hager WH. Hydraulics of embankment weirs. Journal of Hydraulic Engineering, ASCE 1998;124(9):963–71.

[12] Mohamed HI. Flow over gabion weirs. Journal of Irrigation and Drainage Engineering, ASCE 2010;136(8):573–7.

[13] Henderson FM. Open channel flow. New York: Macmillan; 1966.

[14] Brater EF, King HW. Handbook of hydraulics. New York: McGraw-Hill; 1976.

[15] Bos MG. The use of long-throated flumes to measure flows in irrigation and drainage canals. Agricultural Water Management 1977;1:111–26.

[16] Boiten W, Pitlo HR. The V-shaped broad-crested weir. Journal of Irrigation and Drainage Engineering, ASCE 1982;108(2):142–60.

[17] Srivastava R. Flow through open channels. Oxford University, UK: Oxford University Press; 2008: 432.

[18] Jan C, Chang C, Kuo F. Experiments on discharge equations of compound broad-crested weirs. Journal of Irrigation and Drainage Engineering, ASCE 2009;135(4):511–5.

[19] Vatankhah AR, Mahdavi A. Simplified. Flow Measurement and Instrumentation 2012;26:79–84.

[20] Martinez J, Reca J, Morillas MT, Lopez JG. Design and calibration of a compound sharp-crested weir. Journal of Hydraulic Engineering, ASCE 2005;131(2):112–6.

[21] Qu J, Ramamurthy AS, Tadayon R, Chen Z. Numerical simulation of sharp-crested weir flows. Canadian Journal of Civil Engineering 2009;36:1530–4.

[22] Göğüş M, Altınbilek D. Flow measurement structures of compound cross section for rivers. Journal of Irrigation and Drainage Engineering, ASCE 1994;120(1):110–27.

[23] Emamgholizadeh S, Assare K. Investigation of the upstream and downstream slope of the long-throated flumes on the discharge coefficient. Asian Journal of Engineering and Applied Sciences, Research Publishing Network (ARPN) 2008;3(2):62–70.

[24] Atalay AE. Effect of the downstream expansion of a flow measurement flume of rectangular compound cross section on flow properties. Ankara, Turkey: Middle East Technical Univ.; 1992[MS thesis].

[25] Al-Khatib IA. Hydraulic characteristics of flow measurement flumes of rectangular compound cross sections. Ankara, Turkey: Civil Engineering Department, Middle East Technical University; 1989 [MS thesis].

[26] Al-Khatib IA. Hydraulic characteristics and optimum design of Symmetrical compound channels for flow measurements. Ankara, Turkey: Middle East Technical University; 1993 [Ph.D. thesis].

[27] Göğüş M, Al-Khatib I. Flow measurement flumes of rectangular compound cross section. Journal of Irrigation and Drainage Engineering, ASCE 1995;120(1):110–27.

[28] Bos MG, editor. Discharge measurement structures. 3rd revised ed.. Wageningen, The Netherlands: ILRI Publication 20; 1989.

[29] Bos MG, Clemmens AJ, Replogle JA. Flow measuring flumes for open channel systems. New York: Wiley; 1984.

[30] Hatipoglu A.M. Effect of the downstream expansion of a long throated flume of rectangular cross section on flow properties, Civil Engineering Department, Middle East Technical University, Ankara, Turkey, [M.Sc. thesis], 1991.

[31] Bos MG, Reinink Y. Required head loss over long-throated flumes. Journal of Irrigation and Drainage Engineering, ASCE 1981;107(1):87–102.